Available online at www.sciencedirect.com
SCIENCE DIRECT
Journal of Molecular Catalysis A: Chemical 253 (2006) 222–233
JOURNAL OF MOLECULAR CATALYSIS A: CHEMICAL
www.elsevier.com/locate/molcata

Electrochemical reduction of NAD^+ on a polycrystalline gold electrode

Alexis Damian, Sasha Omanovic *

Department of Chemical Engineering and McGill Institute for Advance Materials, McGill University, 3610 University Street, Montreal, Que., Canada H3A 2B2

Received 3 February 2006; received in revised form 12 March 2006; accepted 13 March 2006
Available online 24 April 2006

Abstract

A range of dc and ac electrochemical techniques was used to investigate the kinetics of NAD^+ reduction on a polycrystalline gold electrode surface. It has been shown that the reduction of NAD^+ on gold is irreversible and occurs at cathodic overpotentials larger than −0.2 V. Depending on the reduction potential applied, the ratio between the amount of enzymatically active 1,4-NADH and inactive NAD_2 formed changes from 0.78 at overpotential −0.515 V down to 0.28 at overpotential −0.715 V. The NAD^+ reduction reaction was found to be mass-transport controlled, and of first order with respect to NAD^+. It was shown that the reversible adsorption of NAD^+ reduction reaction products, NAD_2 and NADH, occurs if the stationary electrode is polarized for a longer time in the potential region of NAD^+ reduction, causing electrode fouling. An NAD^+ reduction reaction kinetic model was proposed and successfully validated. A set of kinetic parameters was calculated and verified independently using various experimental techniques: the apparent transfer and diffusion coefficients, the apparent formal heterogeneous electron-transfer rate constant, and the apparent Gibbs energy of activation.

Keywords: NAD^+ reduction; NADH regeneration; Gold electrode; Kinetics; Linear voltammetry; Differential pulse voltammetry; Impedance spectroscopy

1. Introduction

A large number of the biochemical reactions catalyzed by redox enzymes (dehydrogenases or oxidoreductases) are based on the use of nicotinamide adenine dinucleotide NAD(H) (Scheme 1) as a cofactor that plays the role of electron and hydrogen shuttle. In its reduced and enzymatically active form (1,4-NADH), the molecule transfers two electrons and a proton to a substrate in the presence of a suitable enzyme, resulting in the oxidation of NADH to NAD^+. Due to the industrial and biomedical importance of NADH, and also due to its high price, the electrochemical reduction of NAD^+ to NADH (i.e. NADH regeneration) has attracted considerable scientific attention over the years. In order to develop electrochemically based NADH regeneration methods/electrodes, comprehensive knowledge on the mechanisms and kinetics of NAD^+ reduction on various electrode surfaces is required.

Fundamental aspects of the mechanisms and kinetics of NAD^+ reduction have been investigated using mostly bare (non-modified) high-hydrogen-evolution-overpotential electrodes, such as mercury [1–10] and various carbon materials [11]. It has been shown [2–5] that the reduction of NAD^+ on Hg proceeds by the transfer of one electron to the pyridinium ring, but at significantly high cathodic overpotentials (ca. −1.2 V versus SCE at pH 7), followed by fast radical coupling to form an enzymatically inactive dimer NAD_2 (see Scheme 1). The fast dimerization reaction, coupled with the slow second reaction step (electron-transfer and protonation; Scheme 1) is the major reason why the direct reduction of NAD^+ on non-modified electrodes results in the formation of NAD_2, rather than NADH. Only by polarizing the Hg electrode further to extreme cathodic overpotentials (ca. −1.6 V versus SCE), the formed radical could be only partially protonated and further reduced to both 1,4- and 1,6-NADH [4–6]. In addition, the polarographic wave of the second reduction step was observed only in the presence of a surface-active electrolyte. Thus, the direct reduction of NAD^+ on non-modified electrodes results in a low yield of enzymatically active 1,4-NADH [2,6,12].

Therefore, many attempts have been made to modify electrode surfaces in order to increase the kinetics of the second reaction step (electron-transfer and/or protonation; Scheme 1), thus

* Corresponding author. Tel.: +1 514 398 4273; fax: +1 514 398 6678.
E-mail address: sasha.omanovic@mcgill.ca (S. Omanovic).

1381-1169/$ – see front matter © 2006 Elsevier B.V. All rights reserved.
doi:10.1016/j.molcata.2006.03.020

Nomenclature

A	pre-exponential factor in the Arrhenius equation ($A\,cm^{-2}$)
c	concentration ($mol\,cm^{-3}$) or (mM)
C	capacitance ($F\,cm^{-2}$)
C_{dl}	double-layer capacitance ($F\,cm^{-2}$)
CPE	constant phase element ($\Omega^{-1}\,s^{n}\,cm^{-2}$)
D	diffusion coefficient ($cm^2\,s^{-1}$)
E'	formal potential (V)
E_p	peak potential (V)
ΔE	modulation amplitude (V)
F	Faraday constant (96,485 $C\,mol^{-1}$)
ΔG_{act}	apparent formal Gibbs energy of activation ($J\,mol^{-1}$)
$\Delta G_{act,p}$	apparent Gibbs energy of activation determined at a CV or DPV peak potential ($J\,mol^{-1}$)
j	current density ($A\,cm^{-2}$)
j_{ac}	current density calculated from resistance, R ($A\,cm^{-2}$)
j_d	mass-transport (diffusion)-limited current density ($A\,cm^{-2}$)
j_e	electron-transfer current density ($A\,cm^{-2}$)
j_p	peak current density ($A\,cm^{-2}$)
k	apparent heterogeneous electron-transfer rate constant ($cm\,s^{-1}$)
k^f	apparent formal heterogeneous electron-transfer rate constant ($cm\,s^{-1}$)
n	number of electrons
n	exponent of a constant phase element
R	standard gas constant ($8.314\,J\,mol^{-1}\,K^{-1}$)
R	resistance ($\Omega\,cm^2$)
sr	scan rate ($V\,s^{-1}$)
t_m	modulation time (s)
T	temperature (K)
W	Warburg impedance element ($\Omega^{-1}\,s^{1/2}\,cm^{-2}$)
$W_{1/2}$	width of a DPV peak (at half height) (V)
Z	impedance ($\Omega\,cm^2$)

Greek letters

α	apparent transfer coefficient
η	overpotential (V)
θ	surface coverage
τ	time constant (s)
υ	kinematic viscosity ($cm^2\,s^{-1}$)
ω	RDE rotation rate ($rad\,s^{-1}$)

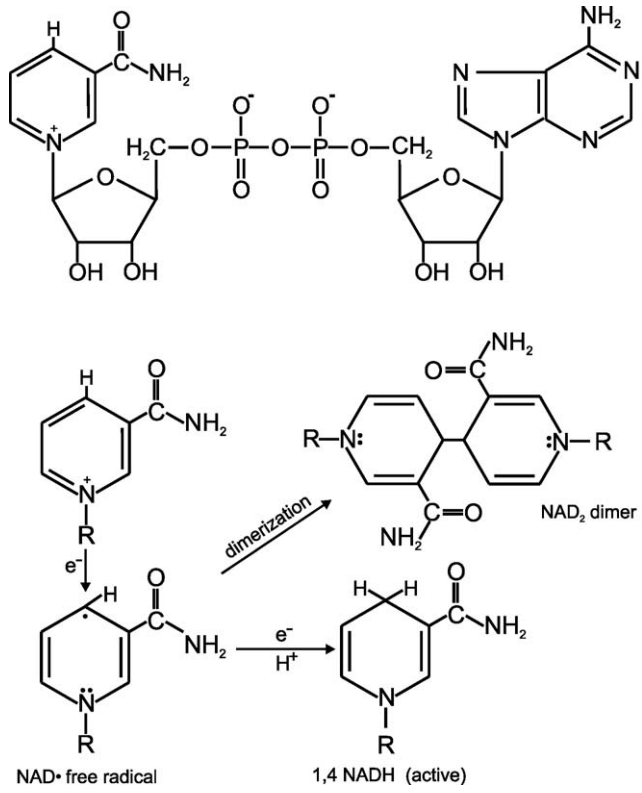

Scheme 1. Nicotinamide adenine dinucleotide in its oxidized form (NAD^+), and its reduction to enzymatically active 1,4-NADH and enzymatically inactive dimer NAD_2. R stands for adenosine diphosphoribose.

preventing the formation of the dimer and enhancing the stereospecificity of the reduction reaction. Electrochemical systems using chemically modified [13–18] and enzyme-mediated electrodes [19–24] have been proposed, and the yield in the active 1,4-NADH produced ranged from ca. 75% on a cholesterol-modified gold–amalgam electrode [13] to ca. 82% on a silver electrode modified with covalently adsorbed L-histidine [14]. We have recently shown that by modifying a glassy carbon electrode surface with nano-islands of electrodeposited ruthenium, a very high yield (96%) of the enzymatically active 1,4-NADH can be formed by the direct reduction of NAD^+ [25,26].

In this paper, we discuss our results on the kinetics of reduction of NAD^+ on a gold electrode using a range of electrochemical techniques. The reason gold has been chosen as an electrode surface is two-fold; firstly, it offers high stability, reproducibility and high hydrogen evolution overpotential, the latest being a condition necessary for studying reduction reactions occurring in aqueous media at potentials more negative than the reversible H^+/H_2 potential. Secondly, gold is an excellent electrode substrate for the surface deposition of: (i) metal nano-islands/particles (e.g. Pt, Pd, Ru) that can provide hydrogen for the second NAD^+ reduction step right at the NAD^+ reduction reaction site (Scheme 1) [25,26], and also for the formation of (ii) self-assembled-monolayers of organic or biomolecules (e.g. alkylthiols, amino-acids, redox enzymes, etc.) that could be potentially used to influence both the kinetics and mechanisms of the NAD^+ reduction reaction in order to increase the yield of the active NADH regenerated [13,14]. To the best of our knowledge, only Takamura et al. [12] have published a study on the reduction of NAD^+ on a polycrystalline gold electrode. However, the paper discusses the interaction of NAD^+ with the Au surface in terms of adsorption, rather than in terms of the reduction kinetics. Here, we report a range of kinetic parameters related to the reduction of NAD^+ on Au.

2. Experimental

The kinetics of the reduction of NAD^+ using a gold electrode was studied in 0.1 M sodium perchlorate pH 5.8 at NAD^+ concentrations varying from 0.65 to 6 mM, and in a wide temperature range, from 295 to 338 K. Chemicals used for the research were purchased from Sigma–Aldrich Company and Fisher Scientifics, and were used without further purification. All solutions were prepared using deionized water (resistivity of 18.2 MΩ cm). A standard three-electrode, two compartment cell was used in all experiments. The counter electrode was a platinum wire of high purity (99.99%, Johnson-Matthey), which was degreased by refluxing in acetone, sealed in soft glass, electrochemically cleaned by potential cycling in 0.5 M sulfuric acid, and stored in 98% sulfuric acid. During the measurement, the counter electrode was separated from the main cell compartment by a glass frit. The reference electrode was a commercially available mercury/mercurous sulfate electrode (MSE; +0.400 V versus SCE), but all potentials in this paper are referred to a saturated calomel electrode (SCE). The working electrode was a polycrystalline gold rotating disc electrode (Autolab-EcoChemie, 3 mm in diameter). Before each experiment the gold electrode was polished with diamond paste down to 3 μm, followed by thorough rinsing with ethanol and cleaning in an ultrasonic bath for 10 min in order to remove polishing residues. The gold electrode was then electrochemically pretreated in 0.5 M perchloric acid by potentiodynamic cyclic polarization between −0.3 and 1.5 V versus SCE at a scan rate of 300 mV s^{-1} for 40 cycles. From scan-dependent cyclic voltammetry measurements made in the double-layer region in 0.5 M perchloric acid, the real surface area of the Au electrode used in the measurements was estimated, and the roughness factor was found to be equal to 1.4. The corresponding values reported in this paper are thus referred (normalized) to the real surface area of the electrode.

All the measurements were carried out in an oxygen-free solution, which was achieved by continuous purging of the cell with argon gas (99.998% pure). All the measurements were made in a quiescent solution, and the inert atmosphere was maintained by saturating the cell space above the electrolyte with argon. The stock NAD^+ solution was prepared in a separate container using the supporting electrolyte. Before measurements in a NAD^+-containing solution, the background response of the electrode was recorded in 0.1 M $NaClO_4$. Aliquots of NAD^+ were then added to the electrochemical cell and the electrochemical measurements were repeated for each aliquot. The NADH activity tests were made according to the regular Sigma Quality Control Test Procedure (EC 1.8.1.4) using lipoamide dehydrogenase (59 U mg^{-1}, Sigma L-2002) as an enzyme and DL-6,8-thioctic acid amide (purity 99–100%, Sigma T-5875) as a substrate.

Electrochemical techniques of linear polarization voltammetry (LP), differential pulse voltammetry (DPV), electrochemical impedance spectroscopy (EIS), and controlled-potential electrolysis were employed using an Ecochemie Autolab potentiostat/galvanostat/frequency_response_analyzer PGSTAT30/FRA2, controlled by the GPES/FRA v.4.9.5 software. EIS measurements involved an ac voltage amplitude of 10 mV (peak to peak) in a frequency range from 50 kHz to 50 mHz. The qualitative and quantitative measurements of the electrolysis products and the enzymatic activity assays were done using a Varian UV–Vis double-beam spectrophotometer.

3. Results and discussion

3.1. Linear polarization and differential pulse voltammetry

Fig. 1a shows the linear polarization voltammograms recorded on a polycrystalline gold electrode in the absence (curve 1) and presence (curve 2) of NAD^+ in the supporting electrolyte. The response in the supporting electrolyte (curve 1) is featureless, and an increase in cathodic current at high negative potentials is related to the hydrogen evolution reaction (HER). On the other hand, a well-defined cathodic peak was recorded at ca. −1.18 V versus SCE in the NAD^+-containing electrolyte (curve 2), indicating that the reduction of NAD^+ occurs in this potential region. Taking into account a pH difference, the NAD^+ reduction peak potential recorded on gold (Fig. 1) is in agreement with the value obtained on a cholesterol-modified gold–amalgam electrode [13], ruthenium-modified glassy carbon (RuGC) electrode [25,26] and basal pyrolytic graphite electrode [27]. Similarly, Moiroux and Elving [11] recorded one cathodic peak at ca. −1.28 V versus SCE on a glassy carbon electrode (GC) in phosphate buffer at pH 7. Takamura et al. [12] observed also one reduction peak on a gold electrode in phosphate buffer pH 8.3, but at lower overpotential, −0.945 V versus SCE. Omanovic and co-workers [25,26] have shown that the cathodic peak on a RuGC electrode corresponds to the two-electron reduction of NAD^+ to NADH (Scheme 1), while Moiroux and Elving [11] interpreted the peak recorded on a bare GC electrode as the reduction of NAD^+ to the NAD_2 dimer (one-electron process).

The result in Fig. 1a (curve 2) also shows that the NAD^+ reduction reaction is highly irreversible, which can be concluded from the potential difference between the first noticeable NAD^+ reduction current (around −0.9 V versus SCE) and formal poten-

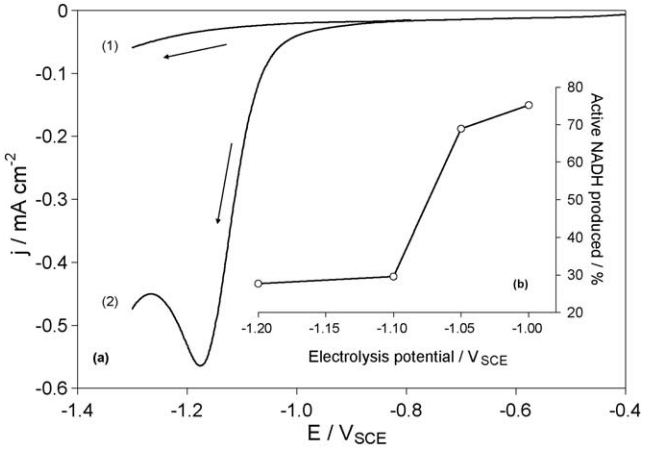

Fig. 1. (a) Linear voltammograms of an Au electrode recorded in (1) 0.1 M $NaClO_4$ and (2) 0.1 M $NaClO_4$ + 5 mM NAD^+. Scan rate, sr = 300 mV s^{-1}. (b) Amount of active 1,4-NADH produced by electrolysis of 700 μM NAD^+ solution at various potentials.

tial of an NAD^+/NADH couple, $E' = -0.485$ V versus SCE at pH 5.8 [28]. This results in NAD^+ reduction overpotential of more than 400 mV. In addition, linear polarization measurements for the oxidation of NADH (not shown here) have demonstrated that the NADH oxidation occurs at potentials higher than 0.55 V versus SCE, thus giving the potential difference (separation) between the NAD^+ reduction and NADH oxidation potential of more than 1.4 V. Therefore, throughout the text, the NAD^+ reduction reaction will be treated as an irreversible electrochemical reaction.

3.1.1. Enzymatic assay—number of electrons involved in NAD^+ reduction

In order to elucidate the NAD^+ reduction reaction mechanisms and kinetics on a gold electrode, a series of scan- and concentration-dependent dc and ac polarization measurements were done. The initial parameter of interest required for the treatment of experimental results is the number of electrons involved in the NAD^+ reduction reaction. However, since the reduction of NAD^+ can result in the formation of both NAD_2 and NADH (Scheme 1), the number of electrons involved in the reduction reaction depends on the relative ratio between the two products formed. Therefore, it was first necessary to determine the relative amount of the two products formed by the reduction of NAD^+ at various reduction potentials.

Fig. 1b shows the dependence of percentage of active NADH formed on the applied NAD^+ reduction potential obtained from potentiostatic reduction experiments. The relative amount of active NADH obtained was determined using a standard enzymatic assay, Sigma Quality Control Test Procedure, EC 1.8.1.4. The observed behavior is quite consistent with the one expected for organic reactions involving the formation of radicals [29]. With an increase in reduction overpotential the amount of active NADH formed decreases, which is due to an increase in the dimerization rate. With an increase in cathodic overpotential, the NAD^+ reduction reaction rate increases, as does the surface amount (coverage) of formed NAD-radicals. Consequently, the probability for two radicals to dimerize also increases. Nevertheless, the amount of active NADH formed at low overpotentials was surprisingly high compared to the available literature data on the direct regeneration of NADH on other non-modified electrodes [2,6,12]. To the best of our knowledge, no literature reporting a potential dependence of the amount of active NADH formed on other electrodes is available, and thus it is not possible to compare the results in Fig. 1b to those obtained by other researchers. However, at reported "optimum conditions", only 10% of active NADH was formed on Au–Hg [13], while a higher yield, 50%, was obtained on Pt [13] and Hg [6]. Our experiments on a Cu electrode [30] have yielded a trend very similar to the one in Fig. 1b, but the highest yield of enzymatically active NADH formed was 73% at −1.0 V, while at −1.2 V a significantly higher amount, 53%, was obtained when compared to the gold electrode (Fig. 1b). Now, taking into account the NAD^+ reduction mechanism (Scheme 1), the data in Fig. 1b can be used to calculate the number of electrons involved in the reduction of NAD^+ on gold in the investigated potential region. Thus, a value of 100% of active NADH formed would indicate that two electrons per one NAD^+ molecule were exchanged in the reaction. On the other hand, 0% of active NADH formed would indicate that one electron per one NAD^+ molecule participated in the reaction, resulting in the formation of only NAD_2. Similarly, 70% of active NADH formed would indicate that 1.7 electrons per one NAD^+ molecule were exchanged in the reduction reaction. Therefore, Fig. 1b enables direct calculation of the number of electrons exchanged in the NAD^+ reduction reaction at each reduction potential applied. The data show that the value ranges from ca. 1.75 at −1.0 V, down to 1.28 at −1.4 V. A sudden change in the curve slope between −1.05 and −1.00 V could be prescribed to the onset of the HER, but the trend observed in the figure will be discussed in more detail in our subsequent paper [30] and is not relevant for the further analysis of results presented in this manuscript.

3.1.2. Transfer coefficient and reaction order

Fig. 2a shows a set of linear polarization voltammograms recorded with increasing scan rate in the potential region of NAD^+ reduction. It is evident that the peak position (potential) shifts towards more negative potential values with an increase in scan rate, thus indicating that the NAD^+ reduction reaction is under the diffusion control [31]. In order to verify this, the dependence between the peak current density (j_p) and square root of scan rate was plotted (Fig. 2b). The graph shows a linear dependence, thus confirming that the reaction is under mass-transport, i.e. diffusion control, under the potentiodynamic conditions applied [32]. However, according to the cyclic voltammetry theory, it has to be noted that the observed mass-transport control applies only to the potential region more negative and including the cathodic peak potential, $E \leq E_p$, while at potentials more positive than E_p, the reaction is most likely under mixed mass- and electron-transfer control.

In order to estimate a value of apparent transfer coefficient, α, the peak potential (E_p) versus logarithm of scan rate (sr) dependence was plotted in Fig. 2c using the LP voltammograms from

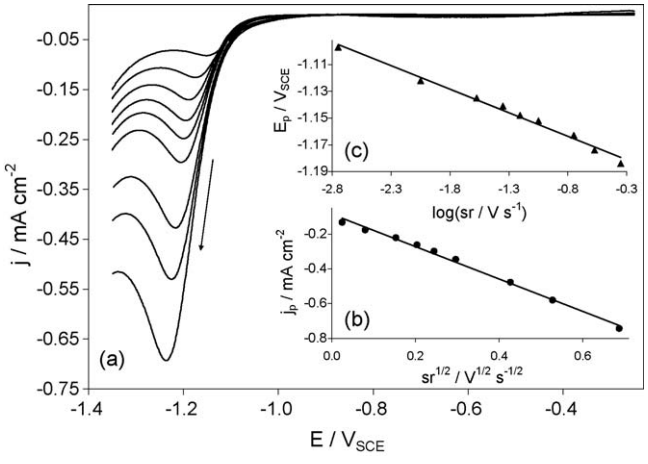

Fig. 2. (a) Linear voltammograms of an Au electrode in 0.1 M $NaClO_4$ + 5 mM of NAD^+ solution recorded at various scan rates. The scan rate increases in the direction of the peak increase as: 2, 10, 30, 50, 70, 100, 200, 300, and 500 mV s^{-1}. Temperature, T = 295 K. Dependence of the peak (b) current and (c) potential on the applied scan rate. The data are obtained from the voltammograms presented in (a).

Fig. 2a. From the slope of the line and applying the relation for an irreversible electrochemical reaction at 295 K [33,34]:

$$\frac{dE_p}{d\log(sr)} = \frac{-0.029}{\alpha n} \quad (3.1)$$

it was calculated that $\alpha n = 0.82$. A very close value, $\alpha n = 0.83 \pm 0.03$, was obtained from the shape factor equation at 295 K [33,34]:

$$|E_p - E_{p/2}| = \frac{0.0472}{\alpha n} \quad (3.2)$$

where $E_{p/2}$ represents the potential of the peak at its half height.

Now, referring to the enzymatic assay data in Fig. 1b, and taking into account that the peak potential values used in the above analysis (Fig. 2a and c) are between −1.1 and −1.2 V versus SCE, the average number of electrons involved in the NAD^+ reduction reaction was calculated to be $n = 1.28$. This gives an apparent transfer coefficient value of $\alpha = 0.64 \pm 0.03$. Burnett and Underwood [1] have reported a value ranging between 0.44 and 0.54, assuming a two-electron NAD^+ reduction process on mercury. In our paper on the reduction of NAD^+ on a ruthenium-modified glassy carbon electrode [25], we have reported a mean value of 0.48.

Further verification of the kinetic data was done by analyzing concentration dependant linear polarization and differential pulse voltammetry experiments. Fig. 3a shows a set of LP voltammograms recorded at various NAD^+ concentrations in the bulk supporting electrolyte. Using the shape factor, Eq. (3.2) and taking that $n = 1.28$, an apparent transfer coefficient value of $\alpha = 0.63 \pm 0.02$ was calculated. This value is in excellent agreement with the value calculated from the scan-dependant LP measurements presented in Fig. 2.

Concentration-dependent measurements were also done using differential pulse voltammetry technique. DPV was chosen as an independent experimental technique offering well-developed mathematical kinetic models that could help us to calculate and verify the same set of kinetic parameters discussed on the basis of LP measurements. Fig. 4a shows a set of DPVs

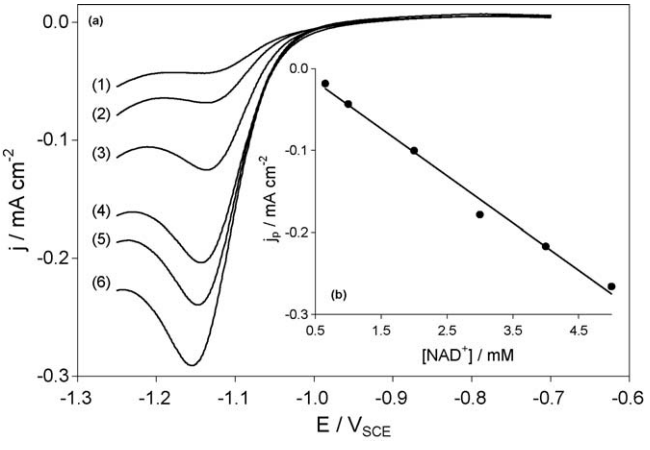

Fig. 3. (a) Linear voltammograms of an Au electrode recorded in 0.1 M $NaClO_4$ containing various concentrations of NAD^+: (1) 0.65 mM, (2) 1 mM, (3) 2 mM, (4) 3 mM, (5) 4 mM, and (6) 5 mM. Scan rate, sr = 100 mV s^{-1}; temperature, $T = 295$ K. (b) Dependence of the peak current on the NAD^+ concentration.

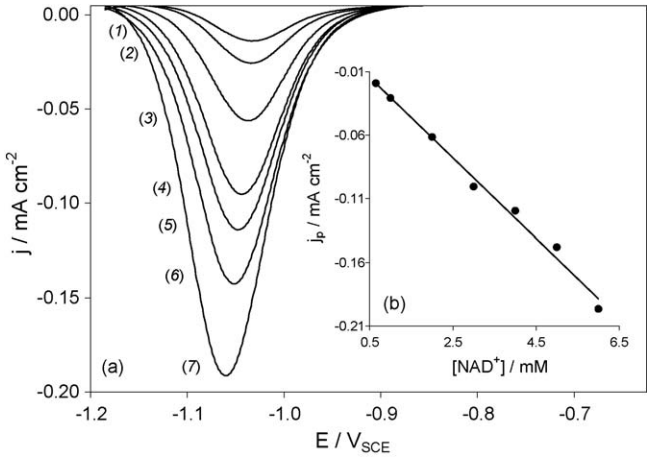

Fig. 4. (a) Normalized differential pulse voltammograms of an Au electrode recorded in 0.1 M $NaClO_4$ containing various concentrations of NAD^+: (1) 0.65 mM, (2) 1 mM, (3) 2 mM, (4) 3 mM, (5) 4 mM, (6) 5 mM, and (7) 6 mM. Modulation time, 70 ms; modulation amplitude, 50 mV; interval time, 0.2 s; step potential, 1.5 mV; scan rate, sr = 7.5 mV s^{-1}; temperature, $T = 295$ K. (b) Dependence of the peak current on the NAD^+ concentration.

recorded in a wide range of concentrations of NAD^+ in the supporting electrolyte. In order to calculate the value of the αn product, the width of the peak at its half height, $W_{1/2}$, was determined at each concentration. Using the equation for an irreversible electrochemical reaction [35,31]:

$$W_{1/2} = \frac{3.52RT}{\alpha n F} \quad (3.3)$$

a mean αn value was calculated to be 0.96 ± 0.04. This value is a little bit higher than the values obtained from the LP voltammetry results. However, considering the potential range where $W_{1/2}$ values were determined, and then referring to the enzymatic assay data in Fig. 1b, the average number of electrons involved in the NAD^+ reduction reaction was calculated to be $n = 1.5$. This in turn yields an apparent transfer coefficient value of $\alpha = 0.64 \pm 0.02$, which is in excellent agreement with the values obtained from the LP measurements. This further verifies the validity of the calculated apparent transfer coefficient values and the applicability of the approaches used in the analysis of the LP and DPV results.

Figs. 3 and 4 demonstrate that the dependence of the peak current on the NAD^+ concentration in the bulk supporting electrolyte is linear, as shown in the insets to the figures. This indicates that the apparent reaction order with respect to NAD^+ is one. Indeed, the observed log–log dependence between the peak current and NAD^+ concentration was found to be linear (LP: $R^2 = 0.9869$, DPV: $R^2 = 0.9982$), with a slope of 0.95 and 1.03 for the LP and DPV results, respectively. This therefore indicates that under the potentiodynamic conditions applied in the LP and DPV measurements, the reduction of NAD^+ on an Au surface follows pseudo first-order kinetics with respect to NAD^+. Very close values (0.99—LP and 1.00—DPV) have been reported in the case of NAD^+ reduction on a ruthenium-modified glassy carbon electrode [25]. Reaction order will again be discussed later in the text, in comparison to the corresponding information obtained from ac impedance measurements.

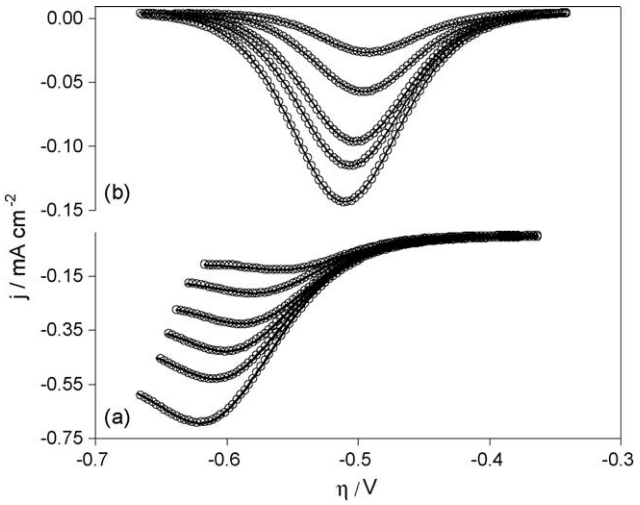

Fig. 5. (a) Experimental (symbol) and simulated (line) LP voltammograms recorded at various scan rates in 0.1 M $NaClO_4$ + 5 mM NAD^+. The scan rate increases in the direction of the peak increase as: 10, 50, 100, 200, 300, and 500 mV s^{-1}. (b) Experimental (symbols) and simulated (line) DP voltammograms recorded in 0.1 M $NaClO_4$ containing various NAD^+ concentrations. The concentration increases in the direction of the peak increase as: 1, 2, 3, 4, and 5 mM. DPV experimental parameters are the same as those in Fig. 4. Temperature, T = 295 K.

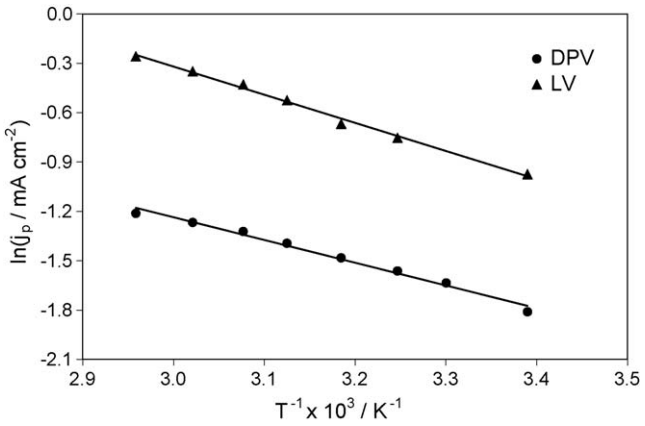

Fig. 6. Temperature variation of peak current obtained from LV and DPV measurements recorded on an Au electrode in 0.1 M $NaClO_4$ + 5 mM NAD^+. (LP) scan rate, sr = 100 mV s^{-1}, (DPV) modulation time, 70 ms; modulation amplitude, 50 mV; interval time, 0.2 s; step potential, 1.5 mV; scan rate, sr = 7.5 mV s^{-1}.

3.1.3. Electron-transfer rate constant and activation energy

As already discussed previously in the text, NAD^+ reduction on a gold electrode is a highly irreversible reaction. Hence, at the formal potential of NAD^+/NADH couple (−0.485 V versus SCE), the corresponding apparent formal heterogeneous electron-transfer rate constant, k^f, is expected to be considerably low. In order to calculate the value of k^f, both LP and DP voltammograms obtained in the wide scan rate and concentration range investigated were fitted by a kinetic model for an irreversible electrochemical reaction using General Purpose Electrochemical System software [36]. Fig. 5 shows that an excellent agreement between the simulated (solid line) and experimental (symbols) voltammograms was obtained for both LP and DPV data. It should be noted that the potential axis in Fig. 5 is presented in terms of overpotential, i.e. it is normalized with respect to the formal potential of the NAD^+/NADH couple (−0.485 V versus SCE at pH 5.8). The mean value of the apparent formal heterogeneous electron-transfer rate constant calculated from scan- and concentration-dependent LP measurements is $k^f = (7 \pm 2) \times 10^{-13}$ cm s^{-1}. A very close value was also obtained from concentration-dependant DPV measurements (Fig. 5b), $k^f = (2 \pm 1) \times 10^{-13}$ cm s^{-1}. Such a low value indicates very slow kinetics of the NAD^+ reduction reaction at the formal potential. The fitting procedure also yielded αn product values, from which the corresponding apparent transfer coefficient was calculated to be $\alpha = 0.70 \pm 0.01$ (LP measurements) and $\alpha = 0.64 \pm 0.02$ (DPV measurements). Both values are in a very close agreement with the values already discussed in the text.

The effect of temperature on the NAD^+ reduction kinetics was also investigated using LP and DPV techniques. It was found that the NAD^+ reduction peak current density increases with an increase in temperature. Fig. 6 demonstrates that this increase obeys the Arrhenius law:

$$j_p = A \exp\left(\frac{-\Delta G_{act}}{RT}\right) \quad (3.4)$$

which enabled us to calculate the apparent Gibbs energy of activation for the reduction of NAD^+ on the Au electrode in the potential region of LP and DPV peaks, $\Delta G_{act,p} = 14.2$ kJ mol^{-1} (LP) and $\Delta G_{act,p} = 11.5$ kJ mol^{-1} (DPV). However, since the Gibbs energy of activation is potential dependent, it is more customary to report its value at a formal potential, ΔG_{act}. The potential dependence of the Gibbs energy of activation is represented as [31]:

$$\Delta G_{act} = \Delta G_{act,p} - \alpha n F \eta \quad (3.5)$$

Using this equation and the corresponding average αn value, the apparent formal Gibbs energy of activation was calculated to be $\Delta G_{act} = 52.8$ kJ mol^{-1} (LP measurements) and $\Delta G_{act} = 51.3$ kJ mol^{-1} (DPV measurements). It is evident that the two values obtained using two different experimental techniques agree very well. They are also close to the value obtained for the reduction of NAD^+ on a ruthenium-modified glassy carbon electrode (59.7 kJ mol^{-1}) [25], and the oxidation of NADH on glassy carbon (60 kJ mol^{-1}) [4]. The obtained apparent formal activation energy value shows that the reduction of NAD^+ is only moderately temperature dependent.

3.2. Hydrodynamic voltammetry

The results discussed previously in the text have been obtained using a stationary Au electrode, and all the measurements were done in a quiescent solution. The kinetic parameters related to the electron-transfer process were calculated. However, the scan-rate-dependent behavior of the peak current density and potential (Fig. 2) indicates that the NAD^+ reduction reaction is under mass-transport control at potentials equal or more positive than the peak potential. Therefore, the

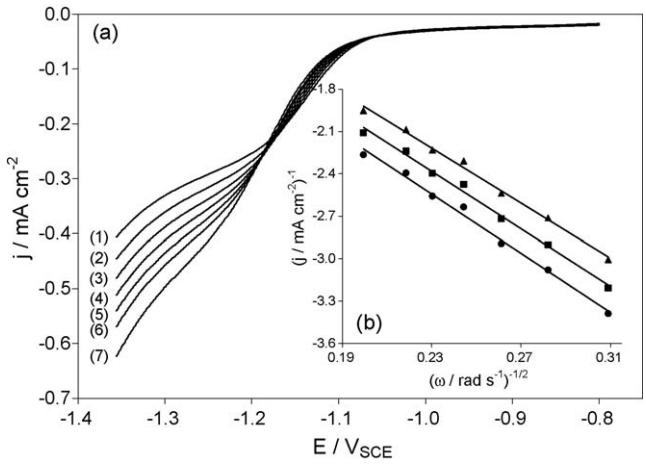

Fig. 7. (a) Steady-state hydrodynamic voltammograms of an Au electrode in 0.1 M $NaClO_4$ + 4 mM NAD^+ recorded at different electrode rotation rates: (1) 100 rpm, (2) 120 rpm, (3) 140 rpm, (4) 160 rpm, (5) 180 rpm, (6) 200 rpm, and (7) 240 rpm. Scan rate, sr = 5 mV s^{-1}; temperature, T = 295 K. (b) Koutecky–Levich plots for the reduction of NAD^+ on an Au electrode obtained from the main plot (a) at different potentials: (●) −1.23 V, (■) −1.25 V, (▲) −1.27 V vs. SCE.

kinetics of the NAD^+ reduction reaction was further studied under convective diffusion conditions. Using an Au rotating disc electrode (RDE) allowed us to separate the contribution of the mass-transport (diffusion of NAD^+ in the solution) from the electron-transfer process. Hence, a value of the diffusion coefficient for NAD^+ in an aqueous solution and an apparent heterogeneous electron-transfer rate constant were calculated. Fig. 7a displays a set of hydrodynamic voltammograms recorded on an Au RDE in 0.1 M $NaClO_4$ + 4 mM NAD^+ at several electrode rotation rates. The observed behavior is in accordance with the one expected for an electrochemical reaction controlled by diffusion in solution. At potentials more positive than ca. −1.17 V versus SCE, the NAD^+ reduction reaction is under mixed (mass-transport/electron-transfer) control, while at potentials more negative than ca. −1.2 V versus SCE, the reaction is under mass-transport control. For the kinetic analysis of the voltammograms, the Koutecky–Levich equation could be used:

$$\frac{1}{j} = \frac{1}{j_e} + \frac{1}{j_d} = \frac{-1}{nFkc} - \frac{1}{0.62nFD^{2/3}\upsilon^{-1/6}c\omega^{1/2}} \tag{3.6}$$

where j is the total (measured) current density at a given potential, j_e the electron-transfer current density, i.e. the current density in the absence of any mass-transport effects, j_d the mass-transport (diffusion)-limited current density, ω the rotation rate of the electrode, υ the kinematic viscosity of the solution (for low-concentration aqueous solutions it is taken to be 0.01 $cm^2\ s^{-1}$), D the diffusion coefficient, c the bulk solution concentration, and k is the potential-dependent apparent heterogeneous electron-transfer rate constant. In order to calculate the diffusion coefficient and apparent heterogeneous electron-transfer rate constant, the dependence between $1/j$ and $1/\omega^{1/2}$ was plotted at several selected potentials in the mass-transport controlled region of the polarization curves (Fig. 7b). Then, taking into account that the average number of electrons exchanged in the NAD^+ reduction reaction in the mass-transport limited potential region is n = 1.27 (Fig. 1b), the values of the diffusion coefficient, D, and apparent heterogeneous electron-transfer rate constant, k, were calculated from the slope and intercept of the lines, respectively. The mean value of D calculated at 295 K is equal to $(1.9 \pm 0.1) \times 10^{-6}$ $cm^2\ s^{-1}$. This order of magnitude indicates that the diffusion of NAD^+ is in the aqueous phase, rather than on the electrode surface, as in the case of NAD^+ reduction on a ruthenium-modified glassy carbon electrode [25,26]. Aizawa et al. [37] obtained a very similar value for the diffusion of NADH in phosphate buffer at 298 K, $D = 2.4 \times 10^{-6}$ $cm^2\ s^{-1}$. Using the Wilke–Chang correlation [38], a semi-theoretical value of the NAD^+ diffusion coefficient was calculated, $D = 3.3 \times 10^{-6}$ $cm^2\ s^{-1}$. This value also agrees well with the value obtained from the RDE measurements (Fig. 7).

Further, from the intercept of the lines in Fig. 7b, a mean value of the apparent heterogeneous electron-transfer rate constant was calculated, $k = (3 \pm 2) \times 10^{-2}$ $cm\ s^{-1}$. Bresnahan and Elving [3] reported roughly an order of magnitude higher value (0.1 $cm\ s^{-1}$) at −1.123 V versus SCE and pH 9.1 on a mercury electrode, assuming that NAD^+ is reduced only to NAD_2 (one-electron process). However, they emphasized that the calculated value is approximate due to uncertainty in determining the value from their reported experimental data.

It would be interesting to compare the k value obtained from the data in Fig. 7 to the apparent formal heterogeneous electron-transfer rate constant, k^f, calculated from LP and DPV measurements. The relation between the two quantities is described by the following equation [34]:

$$k = k^f \exp\left(\frac{-\alpha n F\eta}{RT}\right) \tag{3.7}$$

Using the k values calculated at the three selected overpotentials in the RDE measurements, an average k^f value was calculated to be $(1.2 \pm 0.8) \times 10^{-13}$ $cm\ s^{-1}$. This value is of the same order of magnitude as those obtained from LP and DPV measurements, $(7 \pm 2) \times 10^{-13}$ and $(2 \pm 1) \times 10^{-13}$ $cm\ s^{-1}$, respectively. Hence, this further validates the approaches used to treat the experimental data, as well as their reproducibility and credibility.

3.3. Electrochemical impedance spectroscopy

The electrochemical impedance spectroscopy technique was applied to further investigate the Au electrode/electrolyte interface and the corresponding processes that occur on the Au surface in the presence of NAD^+. To ensure a complete characterization of the interface and surface processes, EIS measurements were made in a wide frequency range, from 50 kHz to 50 mHz, at several selected potentials and NAD^+ concentrations.

3.3.1. Potential-dependant EIS behavior

Fig. 8a shows a set of EIS spectra recorded at several potentials in the absence (triangles) and presence (circles) of NAD^+ in the electrolyte. The spectra are presented in the form of a

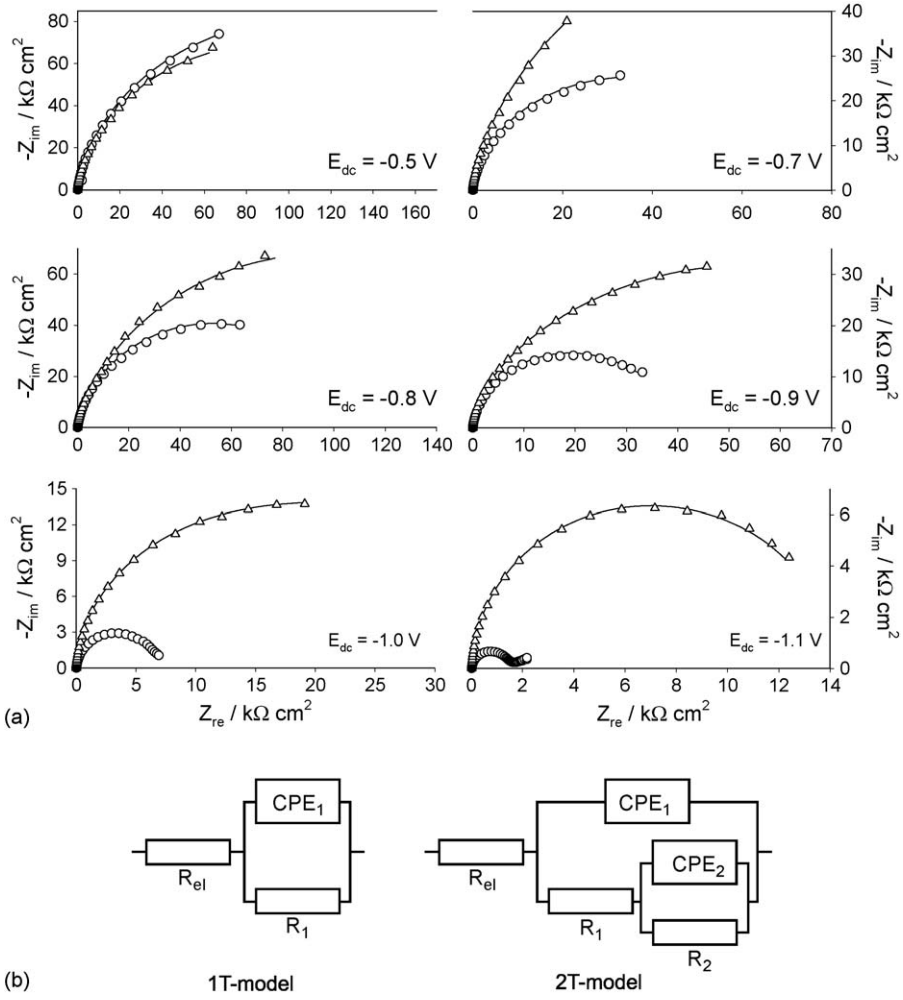

Fig. 8. (a) Nyquist plots of an Au electrode recorded at various dc potentials in (△) 0.1 M $NaClO_4$ and (◯) 0.1 M $NaClO_4$ + 5 mM NAD^+. The solid lines represent the simulated spectra obtained using the equivalent electrical circuit model presented in (b). Temperature, $T = 295$ K. (b) Electrical equivalent circuit used to model the EIS data. EEC code: 1T-model $\equiv R_{el}(Q_1R_1)$ and 2T-model $\equiv R_{el}(Q_1[R_1(Q_2R_2)])$, where $Q \equiv$ CPE, and the corresponding time constants are $\tau_1 = \text{CPE}_1R_1$ and $\tau_2 = \text{CPE}_2R_2$.

complex–impedance (Nyquist) plot. The diameter of the Nyquist plot semi-circle could be, in the first approximation, related to the kinetics of an electrochemical reaction, i.e. it is inversely proportional to the apparent reaction rate. The comparison of the EIS spectra in Fig. 8a and the LP curve recorded in the absence of NAD^+ in the solution (Fig. 1, curve 1) shows that the EIS spectra cover both the double-layer region of the Au electrode (from ca. −0.5 to −0.8 V) and the hydrogen evolution reaction region (negative of −0.8 V). Although the Au electrode is considered to be ideally polarizable in the double-layer region, the semi-circular behavior in Fig. 8a (triangles) clearly shows that there is a finite-rate redox reaction occurring in the double-layer region, and it is the HER. In the absence of a redox reaction, the Nyquist plot would result in a straight vertical line. Obviously, in the HER potential region (negative of −0.8 V) the measured EIS spectra (triangles) correspond to the HER.

However, it is more interesting to compare the relative EIS behavior of the two systems at constant potential, i.e. the response in the presence and absence of NAD^+. Thus, comparison of the two spectra recorded at −0.5 V (Fig. 8a) confirms that no reduction of NAD^+ occurs at this potential since the two spectra overlap. However, at −0.7 V, the extrapolated diameter of the NAD^+ spectrum is significantly smaller than the diameter of the spectrum recorded in the NAD^+-free solution, indicating that the NAD^+ reduction reaction occurs already at this low overpotential, i.e. at overpotential of −0.115 V with respect to the corresponding NAD^+/NADH formal potential. This is not quite visible from the dc linear polarization experiments (Fig. 1), which is due to the different sensitivity of the two techniques. However, as it will be shown later (Fig. 9a), the reduction of NAD^+ at −0.7 V proceeds at a very slow reaction rate, i.e. the relative increase in the total measured reaction rate (with respect to NAD^+-free solution) is only ca. 40%, while, for example, at −1.2 V the increase is 12300%.

In order to quantify the ac impedance behavior of the system, i.e. to relate the observed ac response to a physical picture of the system, the EIS spectra in Fig. 8a were modeled using a non-linear least-squares fit analysis (NLLS) software [39] and

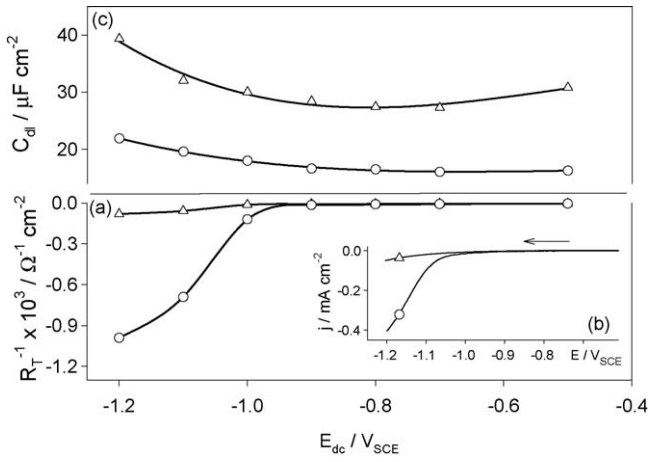

Fig. 9. Dependence of the (a) inverse of total resistance and (c) double-layer capacitance on the applied dc potential obtained by fitting the EIS spectra in Fig. 8. (△) 0.1 M $NaClO_4$ and (◯) 0.1 M $NaClO_4$ + 5 mM NAD^+. In (a) the negative sign of the ordinate is used only to emphasize the cathodic character of the NAD^+ reduction reaction. (b) Steady-state hydrodynamics voltammograms of an Au electrode in (△) 0.1 M $NaClO_4$ and (◯) 0.1 M $NaClO_4$ + 4 mM NAD^+ recorded at the electrode rotation rate of 240 rpm. Scan rate, $sr = 5\,mV\,s^{-1}$; temperature, $T = 295$ K.

an electrical equivalent circuit (EEC). Two different EEC models presented in Fig. 8b have been used to fit the EIS response in the absence and presence of NAD^+ in the electrolyte, a one-time constant model (1T), and a two-time constant model (2T), respectively. In these EECs, R represents the resistance and CPE is the constant phase element. The impedance of a constant phase element is defined as [39] $Z_{CPE} = [CPE(j\omega)^n]^{-1}$, with $-1 \leq n \leq 1$, where the constant CPE is a combination of properties related to both the surface and electroactive species and is independent of frequency. Depending on the value of exponent n, CPE can represents either pure capacitance ($n = 1$), pure resistance ($n = 0$), pure inductance ($n = -1$), or the Warburg (mass-transport) impedance ($n = 0.5$). Deviation of n from the ideal values indicates the presence of inhomogeneities at the microscopic level of the oxide/electrolyte interface (surface roughness, adsorbed species, etc.) [40,41].

Fig. 8a shows that a very good agreement between the experimental (symbols) and simulated (lines) data was obtained when the EEC models in Fig. 8b were used in the fitting, thus confirming the applicability of the proposed EEC models in describing the ac response of the investigated system. The time constant, $\tau_1 = CPE_1R_1$, in the 1T-model describes the response of the HER kinetics on the Au electrode in the supporting electrolyte, namely the charge-transfer resistance, R_1, and double-layer capacitance, CPE_1. The time constant describes the EIS response of the system in the whole frequency region studied. On the other hand, modeling of the spectra recorded in the NAD^+ solution using the 2T-model (Fig. 8b) showed that the first time constant ($\tau_1 = CPE_1R_1$) gives a response in the high-frequency (HF) region, while the response of the second time constant ($\tau_2 = CPE_2R_2$) is located in the low-frequency region (LF). Therefore, the high-frequency time constant can be associated with fast charging/discharging process at the electrode/electrolyte interface, while the low-frequency time constant can be related to mass-transport processes, i.e. the diffusion of NAD^+ from the bulk solution to the electrode surface [31,40,41]. This is in accordance with the hydrodynamic measurements discussed previously in the text. Further, the mean value of n_1 (related to CPE_1) was calculated to be 0.98 ± 0.01 (in the absence of NAD^+) and 0.96 ± 0.01 (in the presence of NAD^+), while $n_2 = 0.44 \pm 0.12$. Hence, it is quite clear that CPE_1 gives the response of a capacitor, and CPE_2 of the Warburg (mass-transport) element. Hence, the meaning of the EEC elements in the 2T-model is the following: constant phase element CPE_1 represents the capacitance related to the electrode/electrolyte interface (double-layer capacitance), R_1 the charge-transfer resistance related to both the NAD^+ reduction and HER, CPE_2 the Warburg (mass-transfer) impedance, and R_2 is the corresponding resistance to mass-transfer. The agreement between the experimental and simulated data in Fig. 8a clearly demonstrates that the proposed EEC models can be successfully used to model the experimental data, giving a physical picture of the electrode/electrolyte interface and corresponding (surface) charge- and mass-transport processes.

It would be interesting to compare the ac behavior of the system to its dc behavior in the potential region presented in Fig. 8a. As shown before, Eq. (3.6), the total current density measured in dc polarization experiments represents the sum of the charge-transfer current density, j_e, and the mass-transport (diffusion) current density, j_d. Similarly, the sum of the charge- and mass-transport resistance, $R_T = R_1 + R_2$, represents the total resistance related to the kinetics of the NAD^+ and hydrogen reduction reaction. Consequently, the inverse value R_T^{-1} could be related to the total current density measured under the potentiostatic conditions, $1/j$. Fig. 9a shows the dependence of R_T^{-1} on the applied dc potential in the supporting electrolyte (triangles) and NAD^+-containing solution (circles). For comparison, the corresponding dc steady-state LP voltammograms are presented in Fig. 9b, and it can be observed that the trend for both plots is very similar. In the absence of NAD^+ in the bulk electrolyte, the measured response using the two techniques is due to the HER. A significant increase in both R_T^{-1} (EIS) and j (LP) is observed when 5 mM of NAD^+ is present in the solution, which is due to the reduction of NAD^+. Hence, R_T^{-1} values could also be used to calculate kinetic parameters related to the NAD^+ reduction reaction, which will be discussed later in the text. Nevertheless, the data presented in Fig. 9a clearly demonstrate that the ac impedance behavior of the system can be well correlated to the corresponding dc voltammetry behavior, which further validates the approach used in the treatment of EIS spectra.

Another EEC parameter of interest is the double-layer capacitance, CPE_1. If the NAD^+ reduction reaction involves an adsorption step (either of the reactant, NAD^+, or the products, NADH and NAD_2), this could be detected by comparing the CPE_1 values recorded in the absence and presence of NAD^+ in the solution. Although the value of the parameter n_1 is close to unity (0.98 ± 0.01 in the absence of NAD^+ and 0.96 ± 0.01 in the presence of NAD^+), its small deviation indicates the presence of surface inhomogeneities, most likely in terms of surface roughness. However, a true value of the double-layer capacitance, C_{dl}, can be conveniently calculated using an equation

originally proposed by Brug et al. [42]:

$$C_{dl} = [CPE_1(R_{el}^{-1} + R_1^{-1})^{n_1-1}]^{1/n_1} \quad (3.8)$$

Fig. 9c shows the potential-dependent behavior of the double-layer capacitance obtained in the absence (triangles) and presence (circles) of NAD^+ in the solution. Although the behavior is very similar in both cases, the values obtained in the NAD^+-containing solution are significantly lower than those obtained in the absence of NAD^+. According to the electrochemical double-layer theory [31], this decrease in the double-layer capacitance indicates that adsorption of reaction species occurs during the NAD^+ reduction reaction. Our electrochemical and PM-IRRAS adsorption measurements done at more positive potentials, where NAD^+ cannot be reduced (from −0.5 to 0.4 V versus SCE) [43], confirmed that NAD^+ is the species that adsorbs on the electrode surface in this *positive* potential region, and that this interaction is spontaneous, strong and irreversible (Gibbs energy of adsorption is $-41 \pm 4\,kJ\,mol^{-1}$, depending on the adsorption potential and temperature). However, since the measurements presented in Fig. 9c were done in the potential region of NAD^+ reduction (except the point at −0.5 V), the evaluation of the surface coverage by NAD^+ under *dynamic* (non-equilibrium) reaction conditions is quite doubtful. Further, our kinetic measurements showed that the adsorption of NAD^+ at −0.5 V is a very slow process, and in the 0.7 mM NAD^+ solution (threshold NAD^+ concentration for the monolayer formation) the equilibrium is reached after ca. 30 min. Hence, it could be safely assumed that: (i) at high NAD^+ reduction overpotentials and (ii) under the experimental conditions applied in the EIS measurements, the electrode surface is not covered by NAD^+ molecules since their reduction is significantly faster than their adsorption. Therefore, the decrease in capacitance observed in Fig. 9c at potentials negative of −0.7 V is due to the surface adsorption of NAD^+ reduction reaction products, namely NADH and/or NAD_2, which results in the electrode surface fouling. This was also noticed during prolonged cyclic polarization of the *stationary* electrode in the potential region of NAD^+ reduction. In these experiments, the NAD^+ reduction current gradually decreased in each subsequent cycle due to the build up of the adsorbed NADH/NAD_2 layer. However, after disconnecting the electrode to the open circuit for a short time, ca. 5 min, the NAD^+ subsequent polarization of the electrode revealed that the reduction current completely recovered to its initial value obtained on the clean electrode surface. This also means that the electrode fouling (i.e. adsorption of NADH and NAD_2) is not permanent, and occurs only when there is a driving force (potential) for the formation and adsorption of NADH/NAD_2. In the absence of the potential driving force (i.e. at an open circuit condition), the formed products quickly desorb and diffuse into the bulk solution. This was further confirmed by cyclic polarization of the rotating disc electrode at high rpm values (1000 rpm). In these experiments no change in the NAD^+ reduction current occurred during the prolonged cyclization of the electrode, indicating that shearing of the adsorbed NADH/NAD_2 layer is enough to overcome the weak attractive coulombic forces and to remove the species off the electrode surface and transport them quickly into the bulk solution.

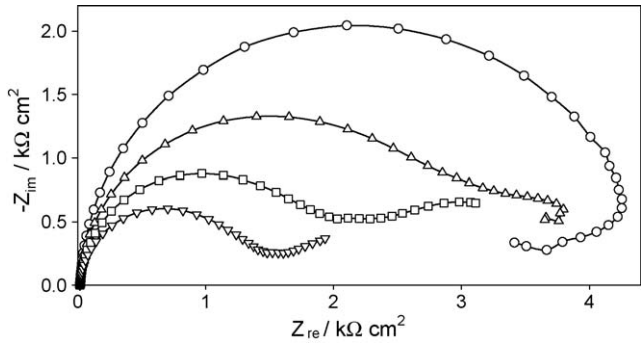

Fig. 10. Nyquist plots of an Au electrode recorded at various concentration of NAD^+ in 0.1 M $NaClO_4$: (◯) 0.5 mM, (△) 1 mM, (□) 2 mM, and (▽) 4 mM. Polarization potential, $E_{dc} = -1.1$ V vs. SCE; temperature, $T = 295$ K.

3.3.2. Concentration-dependant EIS behavior

While in the previous section we discussed the EIS results of the potential-dependant behavior of the NAD^+/Au system, in the following section we will present and discuss results of the NAD^+-concentration-dependant EIS behavior of the system in the potential region of NAD^+ reduction. Fig. 10 shows a set of Nyquist EIS plots recorded at various NAD^+ concentrations at −1.1 V versus SCE. It is obvious that the EIS response changes significantly with changes in NAD^+ concentration in the bulk electrolyte. The spectrum recorded at NAD^+ concentration 0.5 mM (circles) displays a semi-circular behavior in the high- and mid-frequency region. However, in the lowest frequency region a loop-like behavior is recorded. Although the imaginary component of the impedance remains negative, this low-frequency behavior could be related to the inductive response of the system. Such behavior has been shown to originate from the combination of diffusion and adsorption of electroactive species, and the renewal of the electrode surface [44], and is in agreement with the observations obtained from polarization and EIS measurements we already discussed before. Namely, we have shown that the NAD^+ reduction reaction is mass-transport controlled and that the adsorption of the reaction products, NADH/NAD_2, occurs under the potentiostatic conditions of EIS measurements. It is also possible that renewal of the electrode surface occurs due to weak adsorption forces that could be easily overcome either by putting the electrode at open circuit or shearing the electrolyte layer at the electrode surface. Further, the authors in [44] have shown that if the adsorption is slow compared to the diffusion, then the inductive response could be recorded. Therefore, with an increase in the electroactive species concentration in the bulk solution, the adsorption rate is also expected to increase (and the surface coverage). Consequently, the diffusion component of the impedance should start controlling the response in the low-frequency region. Indeed, Fig. 10 shows that with an increase in NAD^+ concentration in the bulk solution, the inductive response of the system gradually disappears while the mass-transport response starts prevailing at low frequencies. The spectrum recorded at NAD^+ concentration 4 mM

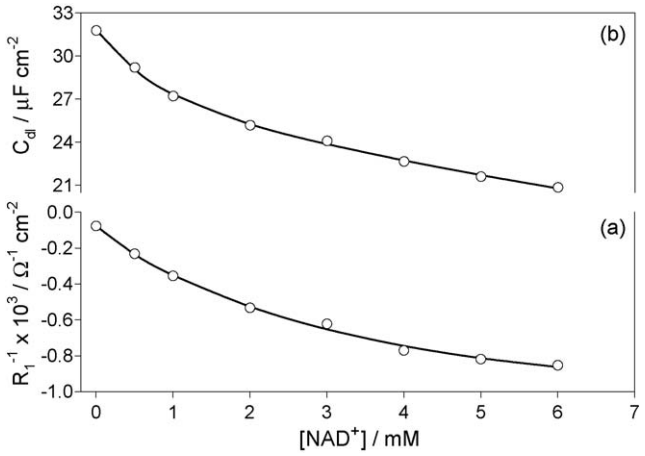

Fig. 11. Dependence of the (a) charge-transfer resistance and (b) double-layer capacitance on the NAD$^+$ concentration obtained by fitting EIS spectra recorded at −1.1 V vs. SCE. In (a) the negative sign of the ordinate is used only to emphasize the cathodic character of the NAD$^+$ reduction reaction.

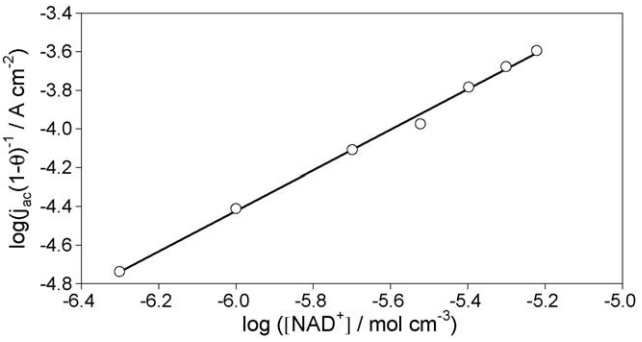

Fig. 12. Relationship between the surface-coverage-corrected current density and NAD$^+$ concentration in the bulk solution obtained from the charge-transfer resistance and double-layer capacitance values presented in Fig. 11.

displays a classical Warburg-tail at low frequencies, indicative of a pure mass-transport control.

Due to the rather complex EIS spectra shape recorded at low NAD$^+$ concentrations, where the inductive response prevails, accurate modeling of the low-concentration EIS data in the entire frequency region was not possible. Hence, only the frequency region corresponding to the semi-circular behavior was modeled using the 1T EEC model in Fig. 8b ($\tau_1 = \mathrm{CPE}_1 R_1$), and the corresponding double-layer capacitance and charge-transfer resistance values were determined and are presented in Fig. 11. The figure shows that with an increase in NAD$^+$ concentration in the bulk electrolyte, the inverse of charge-transfer resistance (which is directly proportional to the kinetic component of the total current density, j_e) also increases (Fig. 11a), while the double-layer capacitance decreases (Fig. 11b). The decrease in the double-layer capacitance indicates that the surface becomes covered with adsorbed species, namely the NAD$^+$ reaction products, NADH and/or NAD_2.

The shape of the two curves in Fig. 11 is very similar and indicates that the reaction rate expressed through the electron-transfer resistance (Fig. 11a) could be dependant on the surface coverage by adsorbed species. Taking into account that the adsorbed species are NADH and/or NAD_2, the following simple kinetic model that describes the rate of the irreversible NAD$^+$ reaction under the potentiostatic conditions applied in the steady-state EIS experiments presented in Fig. 11 could be written:

$$j_{ac} = nFk_{ap}(1-\theta_i)c^z_{NAD^+}c^y_{H^+} \tag{3.9}$$

where c_{H^+} is the concentration of hydrogen ions, y the reaction order with respect to H$^+$, c_{NAD^+} the concentration of NAD$^+$ in the bulk solution, z the reaction order with respect to NAD$^+$, k_{ap} the apparent heterogeneous reaction rate constant, and j_{ac} is the current density (reaction rate) calculated from R_1 using that $j_{ac} \propto 1/R_1$ and $(1-\theta_i)$ is the free electrode surface area available for the NAD$^+$ reduction, where [45]:

$$\theta_i = \frac{C_{dl,0} - C_{dl,i}}{C_{dl,0} - C_{dl,min}} \tag{3.10}$$

In Eq. (3.10), $C_{dl,0}$ is the double-layer capacitance in an NAD$^+$-free solution, $C_{dl,i}$ the double-layer capacitance at a specific (i) concentration of NAD$^+$ in the solution, and $C_{dl,min}$ is the double-layer capacitance at a maximum surface coverage by adsorbed species. Since the capacitance curve in Fig. 11b does not reach a plateau value ($C_{dl,min}$) in the concentration region investigated, $C_{dl,min}$ was evaluated by fitting the curve by an appropriate exponential-decay model, resulting in $C_{dl,min} = 16.13\ \mu F\,cm^{-2}$. Assuming that the concentration of H$^+$ does not change during the EIS experiment, the data in Fig. 11 could be used to test the applicability of Eq. (3.9). The results presented in Fig. 12 shows that the experimental data could be successfully fitted using Eq. (3.9), giving an apparent reaction order with respect to NAD$^+$, $z = 1.05$, and an intercept, $\log(nFc^y_{H^+}k_{ap}) = 1.86$. The obtained reaction order value agrees very well with the values obtained from the potentiodynamic LP and DPV measurements, 0.95 and 1.03, respectively. Also, the obtained intercept agrees well with the corresponding values obtained from Figs. 3b and 4b, 1.56 (LP) and 1.64 (DPV), respectively. However, it should be emphasized that the kinetic model for the fast (and short) *potentiodynamic* LP and DPV measurements differs from the model proposed for long *potentiostatic* EIS measurements, Eq. (3.9). Namely, LP and DPV measurements were done at very short times, using a fresh electrode surface that was kept at open circuit potential for a longer time before the cathodic polarization. No adsorption of NAD$^+$ reduction products was noticed during these measurements. Hence, a kinetic model for potentiodynamic LP and DPV measurements should not include the $(1-\theta_i)$ term from Eq. (3.9). Consequently, the corresponding reaction rate expressed using the peak current density is:

$$j_p = nFk_{ap,p}c^z_{NAD^+}c^y_{H^+} \tag{3.11}$$

The previous analysis and discussion shows that although the kinetic analysis was done using the data obtained from two significantly different types of measurements (short dc potentiodynamic and long ac potentiostatic measurements), a very good agreement between the corresponding kinetic values was

obtained. This confirms the applicability of the proposed kinetic models, Eqs. (3.9) and (3.11), and the assumptions made in establishing the models.

4. Conclusions

A range of dc and ac electrochemical techniques was used to investigate the kinetics of NAD^+ reduction on a polycrystalline gold electrode surface. It was shown that an overpotential of ca. −200 mV is required to initiate the reduction of NAD^+. However, the reaction occurs at an appreciable rate only at cathodic overpotentials larger than ca. −500 mV. Depending on the reduction potential applied, the molar ratio between the amount of enzymatically active 1,4-NADH and inactive NAD_2 formed changes from 0.78 at overpotential −0.515 V, down to 0.28 at overpotential −0.715 V. This is due to an increase in the NAD-radical dimerization rate as a result of an increased surface concentration of formed radicals at higher cathodic overpotentials. Consequently, the number of electrons involved in the NAD^+ reduction reactions also decreases with cathodic overpotential from ca. 1.8 to 1.3. This allowed the determination of the apparent transfer coefficient, $\alpha_{mean} = 0.65$. It was also shown that the high irreversibility and slow kinetics of the NAD^+ reduction reaction at the formal NAD^+/NADH potential is characterized by a very low value of the apparent formal heterogeneous electron-transfer rate constant, $k^f_{mean} = 4 \times 10^{-13}$ cm s^{-1}. Under the experimental conditions employed in dc and ac potentiodynamic and potentiostatic measurements, the reduction of NAD^+ was found to be mass-transport controlled ($D_{mean} = 1.9 \times 10^{-6}$ cm^2 s^{-1}) and of first order with respect to NAD^+. The temperature-dependent measurements yielded an apparent Gibbs energy of activation value of 52.1 kJ mol^{-1} (at the formal NAD^+/NADH potential). It was further shown that the adsorption of NAD^+ reduction reaction products, NAD_2 and NADH, occurs if the stationary electrode is polarized for a longer time in the potential region of NAD^+ reduction, causing electrode fouling. However, the adsorbed products could be easily removed from the surface by shearing the electrolyte close to the electrode surface (using RDE), or by keeping the electrode at open circuit for a short time. A kinetic model that takes into account the adsorption of the NAD^+ reduction reaction products was proposed and successfully validated by the corresponding experimental data.

Acknowledgements

Grateful acknowledgment is made to the Natural Science and Engineering Research Council of Canada for support of this research and Marie-Josee Desroches for editing the text.

References

[1] J.N. Burnett, A.L. Underwood, Biochemistry 4 (1965) 2060.
[2] C.O. Schmakel, K.S.V. Santhanam, P.J. Elving, J. Am. Chem. Soc. 97 (1975) 5083.
[3] W.T. Bresnahan, P.J. Elving, J. Am. Chem. Soc. 103 (1981) 2379.
[4] P.J. Elving, W.T. Bresnaham, J. Moiroux, Z. Samec, Bioelectrochem. Bioenerg. 9 (1982) 365.
[5] J. Moiroux, S. Deycard, T. Malinski, J. Electroanal. Chem. 194 (1985) 99.
[6] H. Jaegfeldt, Bioelectrochem. Bioenerg. 8 (1981) 355.
[7] M.A. Jensen, W.T. Bresnaham, P.J. Elving, Bioelectrochem. Bioenerg. 11 (1983) 299.
[8] C.O. Schmakel, M.A. Jensen, P.J. Elving, Bioelectrochem. Bioenerg. 5 (1978) 625.
[9] W.T. Bresnaham, J. Moiroux, Z. Samec, P.J. Elving, Bioelectrochem. Bioenerg. 7 (1980) 125.
[10] M. Studnickova, H. Paulova-Klukanova, J. Turanek, J. Kovar, J. Electroanal. Chem. 252 (1988) 383.
[11] J. Moiroux, P.J. Elving, J. Electroanal. Chem. 102 (1979) 93.
[12] K. Takamura, A. Mori, F. Kusu, Bioelectrochem. Bioenerg. 8 (1981) 229.
[13] S.H. Baik, C. Kang, I.C. Jeon, S.E. Yun, Biotech. Tech. 13 (1999) 1.
[14] Y.-T. Long, H.-Y. Chen, J. Electroanal. Chem. 440 (1997) 239.
[15] Y. Shimizu, A. Kitani, S. Ito, K. Sasaki, Denki Kagaku 61 (1993) 872.
[16] M. Beley, J.-P. Collin, J. Mol. Catal. 79 (1993) 133.
[17] K. Warriner, S. Higson, P. Vadgama, Mater. Sci. Eng. C5 (1997) 91.
[18] A.A. Karyakin, O.A. Bobrova, E.E. Karyakina, J. Electroanal. Chem. 399 (1995) 179.
[19] A.J. Fry, S.B. Sobolov, M.D. Leonida, K.I. Voivodov, Tetrahedron Lett. 35 (1994) 5607.
[20] K.I. Voivodov, S.B. Sobolov, M.D. Leonida, A.J. Fry, Bioorg. Med. Chem. Lett. 5 (1995) 681.
[21] S.B. Sobolov, M.D. Leonida, A. Bertoszko-Malik, K.I. Voivodov, F. McKinney, J. Kim, A.J. Fry, J. Org. Chem. 61 (1996) 2125.
[22] X. Chen, J.M. Fenton, R.J. Fisher, R.A. Peattie, J. Electrochem. Soc. 151 (2004) E56.
[23] S. Kim, S.-E. Yun, C. Kang, Electrochem. Commun. 1 (1999) 151.
[24] S. Kim, S.-E. Yun, C. Kang, J. Electroanal. Chem. 465 (1999) 153.
[25] F. Man, S. Omanovic, J. Electroanal. Chem. 568 (2004) 301.
[26] A. Azem, S. Omanovic, J. Mol. Catal. A: Chem. 219 (2004) 283.
[27] Y. Nakamura, S.-I. Suye, J.-I. Kira, H. Tera, I. Tabata, M. Senda, Biochem. Biophys. Acta 1289 (1996) 221.
[28] W.M. Clark, Oxidation Reduction Potentials of Organic Systems, Williams & Wilkins, Baltimore, 1960.
[29] C.H. Hamann, A. Hamnett, W. Vielstich, Electrochemistry, Wiley-VCH, Germany, 1998.
[30] A. Damian, K. Maloo, S. Omanovic, in preparation.
[31] A.J. Bard, L.R. Faulkner, Electrochemical Methods: Fundamentals and Applications, second ed., Wiley, 2001.
[32] S. Sampath, O. Lev, J. Electroanal. Chem. 446 (1998) 57.
[33] R.S. Nicholson, I. Shain, Anal. Chem. 36 (1964) 706.
[34] J.-P. Diard, B. Le Gorrec, C. Montella, Cinétique Électrochimique, Hermann, Paris, 1996.
[35] E.P. Parry, R.A. Osteryoung, Anal. Chem. 37 (1965) 1635.
[36] Eco Chemie B.V., General Purpose Electrochemical system, Version 4.9.5.
[37] M. Aizawa, R.W. Coughlin, M. Charles, Biochim. Biophys. Acta 385 (1975) 362.
[38] H.S. Fogler, Elements of Chemical Reaction Engineering, third ed., Prentice Hall, 1999.
[39] B.A. Boukamp, Equivalent Circuit Users Manuel, Report CT88/265/128, University of Twente, Department of Chemical Technology, The Netherlands, 1989.
[40] S. Omanovic, S.G. Roscoe, Langmuir 15 (1999) 8315.
[41] S. Omanovic, S.G. Roscoe, J. Colloid Interface Sci. 227 (2000) 452.
[42] G.J. Brug, A.L.G. Van Der Eeden, M. Sluyters-Rehbach, J.H. Sluyters, J. Electroanal. Chem. 176 (1984) 275.
[43] A. Damian, S. Omanovic, in preparation.
[44] J. Bressan, R. Wiart, J. Electroanal. Chem. 107 (1980) 233.
[45] B.B. Damaskin, O.A. Petrii, V.V. Batrakov, Adsorption of Organic Compounds on Electrodes, Plenum Press, New York, 1971.